Chinese Journal of
POLYMER SCIENCE

RESEARCH ARTICLE

https://doi.org/10.1007/s10118-026-3734-2
Chinese J. Polym. Sci.

Anisotropic Hydrogels with Aligned Porous Structures for Light-steerable Autonomous Rolling

Jia-Xin Yu, Xin Yao*, Ru-Yu Zheng, and Huai-Ping Cong*

Anhui Province Engineering Research Center of Flexible and Intelligent Materials, School of Chemistry and Chemical Engineering, Hefei University of Technology, Hefei 230009, China

Electronic Supplementary Information

Abstract Hydrogel actuators with intrinsic softness, biocompatibility and large deformability hold great promise for extensive applications in intelligent autonomous soft robotics. However, achieving directionally controllable autonomous motion under constant stimulation remains a key challenge, primarily due to the isotropic and densely crosslinked nature of conventional hydrogel networks, which limits both directional driving forces and efficient mass transport pathways. Here, we report a simple method for the fabrication of curved cylindrical hydrogels with aligned porous channels that enable autonomous rolling under constant light irradiation *via* directional freezing assembly-assisted *in situ* photopolymerization. Benefiting from the oriented open-cell network, the hydrogel exhibited fast light-responsive deformation with bending and recovery speeds of 16.5 (°)·s^{-1} and 24 (°)·s^{-1}, respectively. Notably, the hydrogel achieved self-sustained rolling under constant light irradiation at a speed of 0.77 mm·s^{-1}, arising from the synergy of structural anisotropy and geometric curvature. By spatially modulating the irradiation region, the photo-guided direction-steerable rolling could be realized. Additionally, the hydrogel implemented multiple tasks including obstacle crossing, stair climbing and cargo transport, highlighting its potential in biomimetic soft robotic systems.

Keywords Anisotropic hydrogel; Self-sustained locomotion; Directional freezing assembly; Aligned porous structure; Soft robots

Citation: Yu, J. X.; Yao, X.; Zheng, R. Y.; Cong, H. P. Anisotropic hydrogels with aligned porous structures for light-steerable autonomous rolling. *Chinese J. Polym. Sci.* https://doi.org/10.1007/s10118-026-3734-2

INTRODUCTION

Autonomous intelligent soft robots, characterized by inherent flexibility, safe interactive capability, and adaptability to complex environments, are highly attractive in the fields of medical rehabilitation,[1] intelligent agriculture[2,3] and man-machine interaction.[4–6] Stimuli-responsive hydrogels with exceptional softness, biocompatibility, and large reversible shape changes[7,8] are promising candidates for constructing autonomous locomotion systems under constant stimulation.[9–11] Among various external stimuli, light is distinguished by its non-invasiveness, remote controllability, and contactless manipulation and facilitates autonomous locomotion by inducing self-shadowing effects.[12–15] A photo-responsive hydrogel achieves continuous self-oscillation under constant light irradiation by establishing a negative feedback loop *via* phototropic bending and further enables sustained autonomous swimming locomotion.[16] However, constrained by isotropic and homogeneous polymer networks, conventional hydrogels fail to generate asymmetric driving forces under external uniform and constant stimuli, resulting in locomotion directions that are highly dependent on the applied external stimuli, as well as insufficient locomotion sustainability and controllability under continuous stimulation.[16–18]

Inspired by the highly oriented architectures in biological systems (such as pine cones,[19] muscle fibers[20] and motile microorganisms[21]), the construction of anisotropic structures in hydrogel networks can endow hydrogels with asymmetric deformation, enabling them to continuously generate net torque upon interaction with the external environment, thus facilitating autonomous directional locomotion. The ice-templating technique serves as an effective strategy for simultaneously constructing anisotropic architectures and interconnected open porous channels within hydrogel matrices, which effectively accelerates mass transport and improves the actuation response speed of hydrogel-based soft actuators.[22–24] In addition, tailored geometric shapes (*e.g.*, curved cylinders) can actively break the spatial geometric symmetry under external stimuli, thereby generating a directional driving force to initiate and sustain rolling locomotion.[25] Thus, the integration of well-organized oriented porous structures and optimized macroscopic geometric shapes provides a feasible and efficient approach to realize continuous autonomous motion under constant light stimu-

* Corresponding authors, E-mail: xinyao@hfut.edu.cn (X.Y.)
E-mail: hpcong@hfut.edu.cn (H.P.C.)
Special Topic: Functional Gels
Received April 1, 2026; Accepted May 5, 2026; Published online August 3, 2026

lation.

Herein, we reported a facile strategy for fabricating curved cylindrical hydrogels with aligned porous channels *via* directional freezing-assisted *in situ* photopolymerization, enabling autonomous rolling under constant light irradiation. Benefiting from the anisotropic structure and oriented open-cell network, the cylindrical hydrogel exhibited rapid anisotropic deformation, with a shrinkage ratio of 0.21 in the length direction within 2.1 s, which was twice that in the diametral direction. Under light irradiation, the hydrogel rapidly bent to 48° within 2.9 s and fully recovered to its initial shape within 2 s after light removal. Notably, the curved cylindrical gels achieved continuous directional self-rolling under constant light irradiation with a speed of 0.77 mm·s^{-1} enabled by the synergistic effect of intrinsic oriented porous structures and geometric curvature. Photo-guided direction-steerable rolling could be realized by regulating the irradiated region on the hydrogel. Additionally, the hydrogel implemented multiple tasks, including obstacle crossing, stair climbing and cargo transportation under constant light stimulation, holding great potential in biomimetic smart soft robotics.

EXPERIMENTAL

Materials

N-isopropylacrylamide (NIPAM, monomer) was purchased from TCI (Shanghai) Development Co., Ltd. *N,N'*-methylenebis(acrylamide) (MBA, crosslinking agent), glycerol, silver nitrate ($AgNO_3$) and sodium chloride (NaCl) were obtained from Sinopharm Chemical Reagent Co., Ltd. 2-Hydroxy-2-methylpropiophenone (1173, photoinitiator) was purchased from Shanghai Aladdin Biochemical Technology Co., Ltd. Polyvinylpyrrolidone (PVP) was purchased from Sigma-Aldrich (Shanghai) Trading Co., Ltd. Milli-Q purified water was used for all experiments.

Synthesis of Silver Nanowires (AgNWs)

PVP (10 g) and glycerol (400 mL) were uniformly mixed by stirring, followed by heating in an oven at 160 °C for 10 min until PVP was fully dissolved and the solution became transparent. After cooling to room temperature, aqueous solutions of $AgNO_3$ (5 g, dissolved in 3 mL of H_2O) and NaCl (300 mg, dissolved in 2 mL of H_2O) were sequentially added under continuous stirring. The mixture was then heated in an oven at 180 °C for 16 h. After the solution turned grayish green and cooled down naturally, the AgNW precipitate was repeatedly washed with deionized water to obtain a pure AgNW dispersion.

Synthesis of Anisotropic Hydrogels

The precursor solution was prepared by uniformly mixing the NIPAM of 16.4 wt%, MBA of 0.61 wt%, photoinitiator 1173 of 1.02 wt%, and AgNWs of 0.82 wt%. After being placed in a low-temperature environment for 10 min, the precursor solution was filled into curved silicone tubes with an inner diameter of 1 mm. The tubes were then rapidly transferred to a metal plate at –60 °C in a liquid nitrogen bath. After the solution was completely frozen, the precursor was immediately polymerized under 365 nm ultraviolet (UV) irradiation for 2 min. Finally, the as-prepared hydrogel was demolded from the silicone tube and soaked in deionized water to remove unreacted residual monomers.

Characterizations

Transmission electron microscopy (TEM, H-7650) and scanning electron microscopy (SEM, SU8020) were used to characterize the morphology of the AgNWs. Structural and compositional analyses of the hydrogels were performed using SEM and elemental mapping on a Zeiss Merlin Compact field-emission scanning electron microscope equipped with an Oxford Inca energy instrument at an acceleration voltage of 5 kV. The mechanical properties of the hydrogels in the equilibrated state were measured at room temperature using an Instron 5965A testing instrument with a stretch speed of 20 mm·min^{-1}. The stimuli-responsive deformation of the hydrogel was recorded using a camera and analyzed by measuring the variations in the dimensions and bending angle of the gel. The relative dimensional change was calculated using the formulas $(L_0–L_t)/L_0$ and $(D_0–D_t)/D_0$, where L_0 and D_0 represent the initial length and diameter, respectively, and L_t and D_t denote the length and diameter after deformation, respectively. Shrinkage ratios were calculated as L_t/L_0 and D_t/D_0. In addition, the bending response and recovery speeds were determined using the equation $(\alpha_t-\alpha_0)/t$, where α_0 is the initial bending angle, α_t is the angle after deformation, and t is the response or recovery time.

RESULTS AND DISCUSSION

A simple method of directional-freezing-induced assembly-assisted *in situ* polymerization was developed to fabricate a fast-responsive hydrogel with an anisotropically oriented porous structure. As illustrated in Fig. 1, the polymerizable precursor solution containing NIPAM and AgNWs was filled into a preformed curved silicone tube, and the directional freezing assembly was carried out along the direction parallel to the diameter of the tube at –60 °C (Fig. S1 in the electronic supplementary information, ESI). During the freezing process, the directional growth of ice crystals induced the assembly of the AgNWs into an orderly arranged and interconnected 3D network structure (Fig. S2 in ESI). Following cryo-photopolymerization, an anisotropic porous PNIPAM/AgNWs (APPA) hydrogel with 3D interconnected, open and oriented channels was successfully fabricated. The top-view SEM images showed a typical honeycomb-like network with a pore size of about 27 μm, where secondary micropores were distributed on the pore walls (Figs. 2a–2c and Fig. S3a in ESI). Parallel to the growth direction of ice crystals, a highly oriented lamellar structure with a lamellar spacing of approximately 7 μm was observed, where the neighboring lamellae were interconnected and formed an interconnected secondary network (Figs. 2d–2f and Fig. S3b in ESI). Uniform distributions of Ag, C, O and N in the elemental mappings confirmed the incorporation of AgNWs within the PNIPAM crosslinking network (Fig. S4 in ESI). For comparison, an isotropic porous PNIPAM/AgNWs (IPPA) hydrogel prepared by random freezing in a refrigerator and subsequent photopolymerization showed a uniform and disordered porous structure with pore sizes of about 9 μm (Fig. S5 in ESI). Another control PNIPAM/AgNWs (PA) hydrogel prepared by *in situ* polymerization exhibited an irregular, closed and isotropic network with a pore size of about 2 μm (Fig. S6 in ESI). Benefiting from the highly ordered assembled architecture that facilitated stress dispersion along oriented channels and dissipated energy *via* synergistic deformation of interconnected pore walls, the APPA hydrogel exhib-

ited a significantly enhanced mechanical performance, reaching a tensile stress of 16 kPa at 122% strain compared to 5 kPa at 62% strain for the isotropic PA hydrogel (Fig. S7 in ESI).

Owing to its highly anisotropic structure with open interconnected porous microchannels, the APPA hydrogel exhibited fast and anisotropic deformation when exposed to exter-

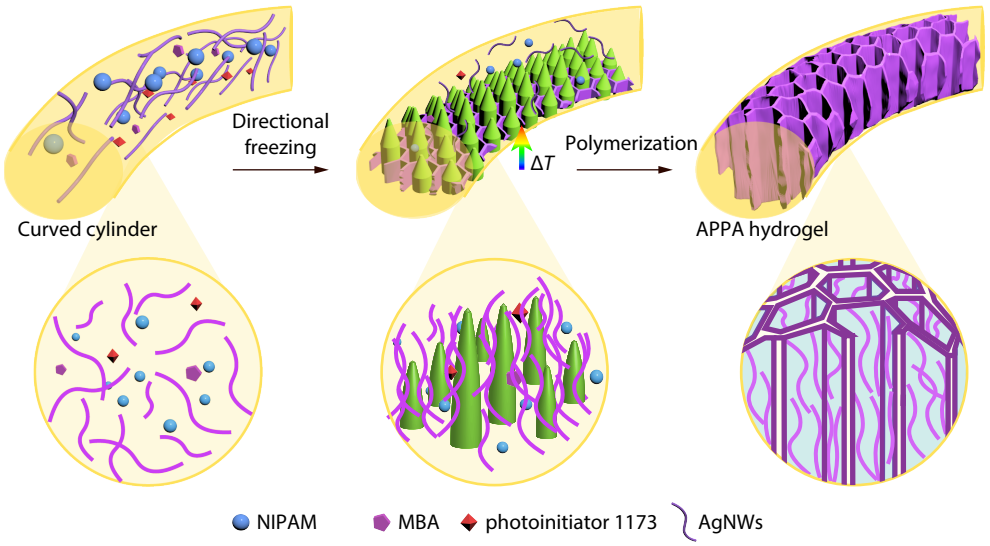

Fig. 1 Fabrication of the APPA hydrogel. The precursor solution containing NIPAM, MBA, photoinitiator 1173, and AgNWs was filled into a curved silicone tube, and directional freezing was applied to construct an aligned porous architecture. Through the subsequent cryo-photopolymerization, the curved cylindrical APPA hydrogel with open oriented porous channels was obtained.

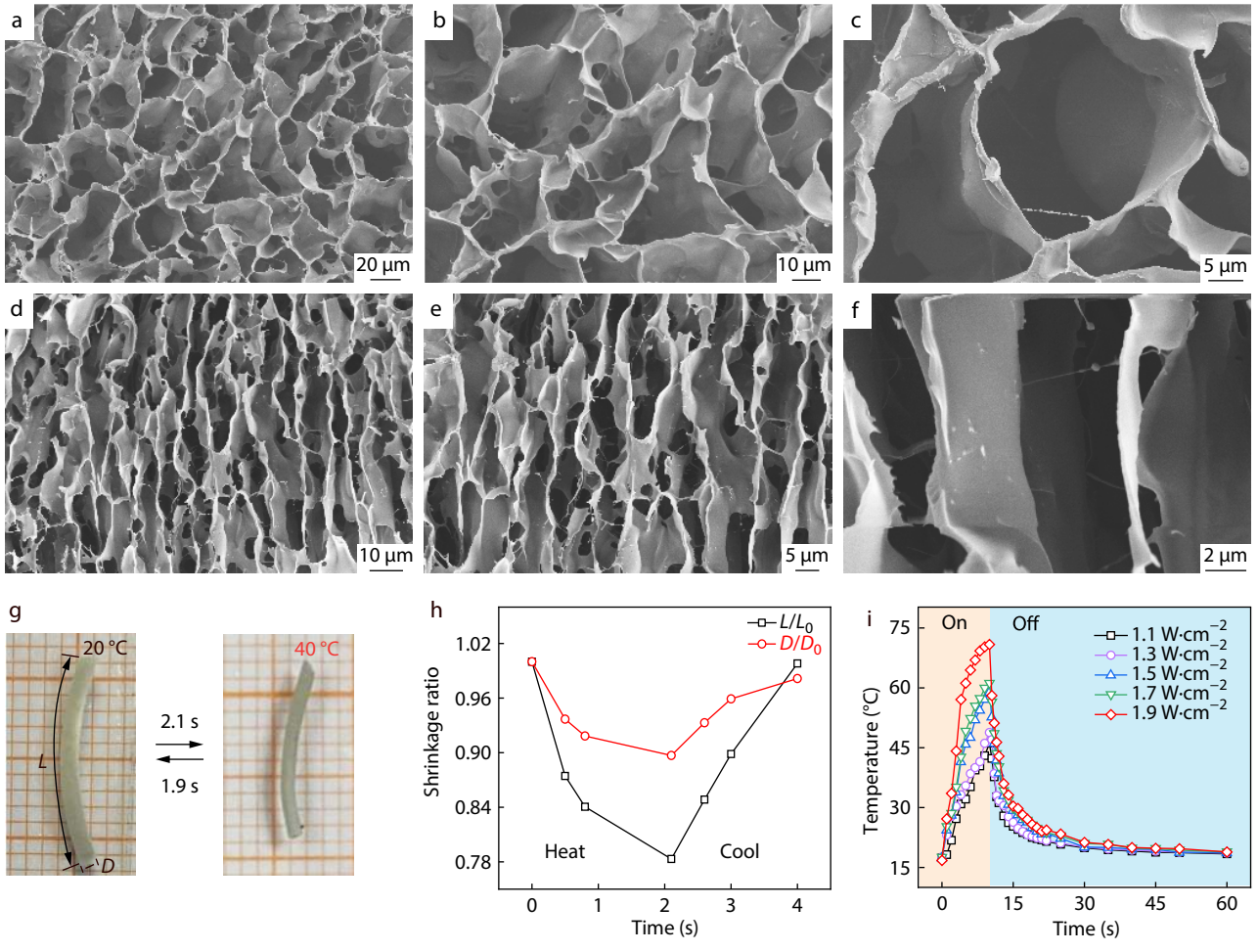

https://doi.org/10.1007/s10118-026-3734-2

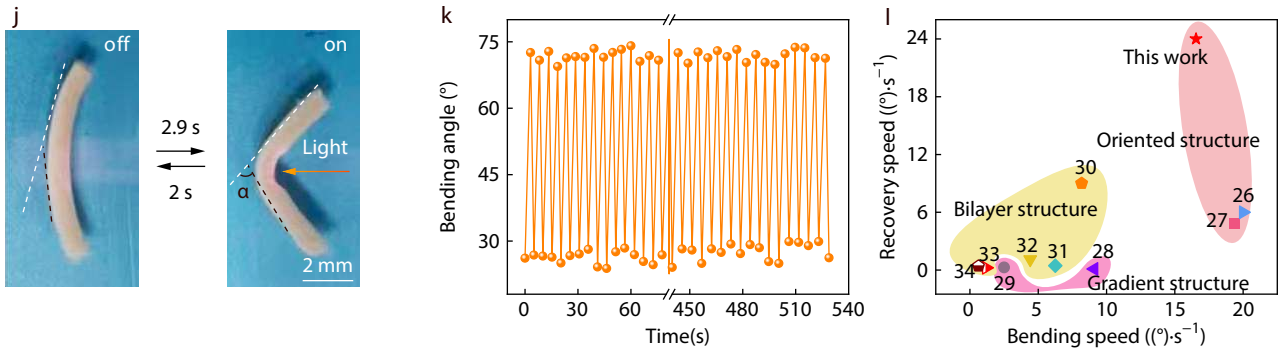

Fig. 2 Structural characterizations and stimuli-responsive performances. (a–f) SEM images with different magnifications of the APPA hydrogel: top view (a–c); side view (d–f). (g) Optical images of the thermo-responsive deformation of the APPA hydrogel. (h) Dimensional variations of the APPA hydrogel as a function of time in water baths at 40 and 20 °C. *L* and *D* represented the length and the diameter, respectively. (i) Temperature variations of the APPA hydrogel under NIR irradiation at different laser intensities; (j) Optical images of the photo-responsive bending deformation of the APPA hydrogel under NIR irradiation at 1.9 W·cm^{-2}; (k) Cyclic stability curve of bending deformation of the APPA hydrogel for 100 cycles; (l) Comparison of the photo-responsive deformation and recovery rates (bending angle divided by deformation/recovery time) of the APPA hydrogel with previously reported works.[26–34]

nal stimuli. When immersed in a 40 °C water bath, which was higher than the lower critical solution temperature (LCST) of PNIPAM, the APPA hydrogel rapidly contracted by 21.7% in the longitudinal direction within 2.1 s, which was 2 times than in the radial direction (Figs. 2g and 2h). Once transferred into a water bath at 20 °C, the shrunken hydrogel immediately absorbed water and expanded to its original shape within 1.9 s. In contrast, the control IPPA hydrogel exhibited rapid yet isotropic responsiveness, achieving a shrinkage ratio of 30% within 3.5 s in hot water and recovering its original state within 3.4 s in cold water (Fig. S8 in ESI). The PA hydrogel, with a disordered and dense structure, exhibited isotropic deformation under thermal stimulation, with a recovery time of 5 min (Fig. S9 in ESI). Benefitting from the efficient photothermal conversion of the well-assembled AgNWs, the APPA hydrogel exhibited rapid photo-responsive deformation. Upon irradiation with an 808 nm near-infrared (NIR) light at a power density of 1.7 W·cm^{-2}, the local temperature of the irradiated region of the APPA hydrogel rapidly increased from 14 °C to 72 °C within 10 s, far exceeding the LCST of PNIPAM (Fig. 2i). In addition, owing to the limited penetration depth of NIR light, a remarkable temperature difference of up to 13 °C was observed between the irradiated and non-irradiated sides, yielding a stable radial temperature gradient in the curved cylindrical hydrogel (Fig. S10 in ESI). After 2.9 s of irradiation, the cylindrical APPA hydrogel bent toward light by 48° owing to the asymmetric thermal strain caused by the radial temperature gradient (Fig. 2j and Fig. S11 in ESI). Upon turning off NIR light, the hydrogel rapidly recovered to its initial state within 2 s. It was observed that hydrogel diameter had a significant impact on bending deformation. As the hydrogel diameter increased from 0.8 mm to 2.0 mm, both the bending speed and maximum bending angle decreased because hydrogels with larger diameters exhibited a weaker photothermal gradient (Fig. S12 in ESI). The optimal bending performance occurred at a diameter of 0.8 mm, resulting in a bending angle of 55° due to sufficient light penetration and a pronounced through-thickness temperature gradient. Furthermore, after 100 deformation cycles, the deformation and recovery speeds decreased slightly from 16.5 (°)·s^{-1} to 11 (°)·s^{-1} and from 24 (°)·s^{-1} to 22 (°)·s^{-1}, respectively, demonstrating excellent reversibility and cycling stability (Fig. 2k). To investigate the structural stability of the APPA hydrogel, microstructural changes were observed before and after 100 consecutive light-driven deformation-recovery cycles. After 100 cycles of photo-actuation, the hydrogel maintained a well-preserved porous network and aligned channels with no observable cracks or pore collapse (Fig. S13 in ESI). The excellent structural stability of the APPA hydrogel could be primarily attributed to the well-assembled 3D AgNW scaffold and the oriented porous structure fabricated by directional freezing, which effectively dispersed and buffered stress concentrations during cyclic deformation, thereby preventing structural damage caused by excessive local stress. The average deformation and recovery speeds were measured to be 16.5 (°)·s^{-1} and 24 (°)·s^{-1}, respectively, outperforming most previously reported thermally actuated hydrogels (Fig. 2l).

Notably, the APPA hydrogel exhibited sustained and directional self-rolling when vertically irradiated at the center of the curved cylinder (Fig. 3a). Initially, the gravitational force (*G*) and the supporting force (F_N) from the substrate were uniformly distributed along the longitudinal direction of the curved cylindrical hydrogel placed on a planar substrate (Fig. S14a in ESI). When NIR light irradiated the centroid of the hydrogel, it rapidly bent and lifted the two ends, causing the F_N to gradually concentrate toward the center of the cylinder. Driven by the geometric curvature of the gel, *G* and the redistributed F_N formed a torque (τ) that propelled the gel to roll toward its concave side (Fig. 3a-i and Fig. S14b in ESI). Once rolling commenced, the irradiation region was autonomously refreshed, while the persistent temperature difference between the irradiated and unirradiated sides ensured the self-sustaining rolling behavior of the gel (Figs. 3a-ii–3a-iv). During autonomous rolling of the APPA hydrogel, the centroid exhibited a continuous horizontal displacement along the *X*-axis (from 0 mm to 25 mm), accompanied by periodic vertical fluctuations in the *Y*-direction (approximately from 0.7 mm to 1.2 mm) (Fig. S15 in ESI). This typical motion trajectory of the centroid was closely related to the deformation behavior of the hydrogel during the rolling process. Impressively, a

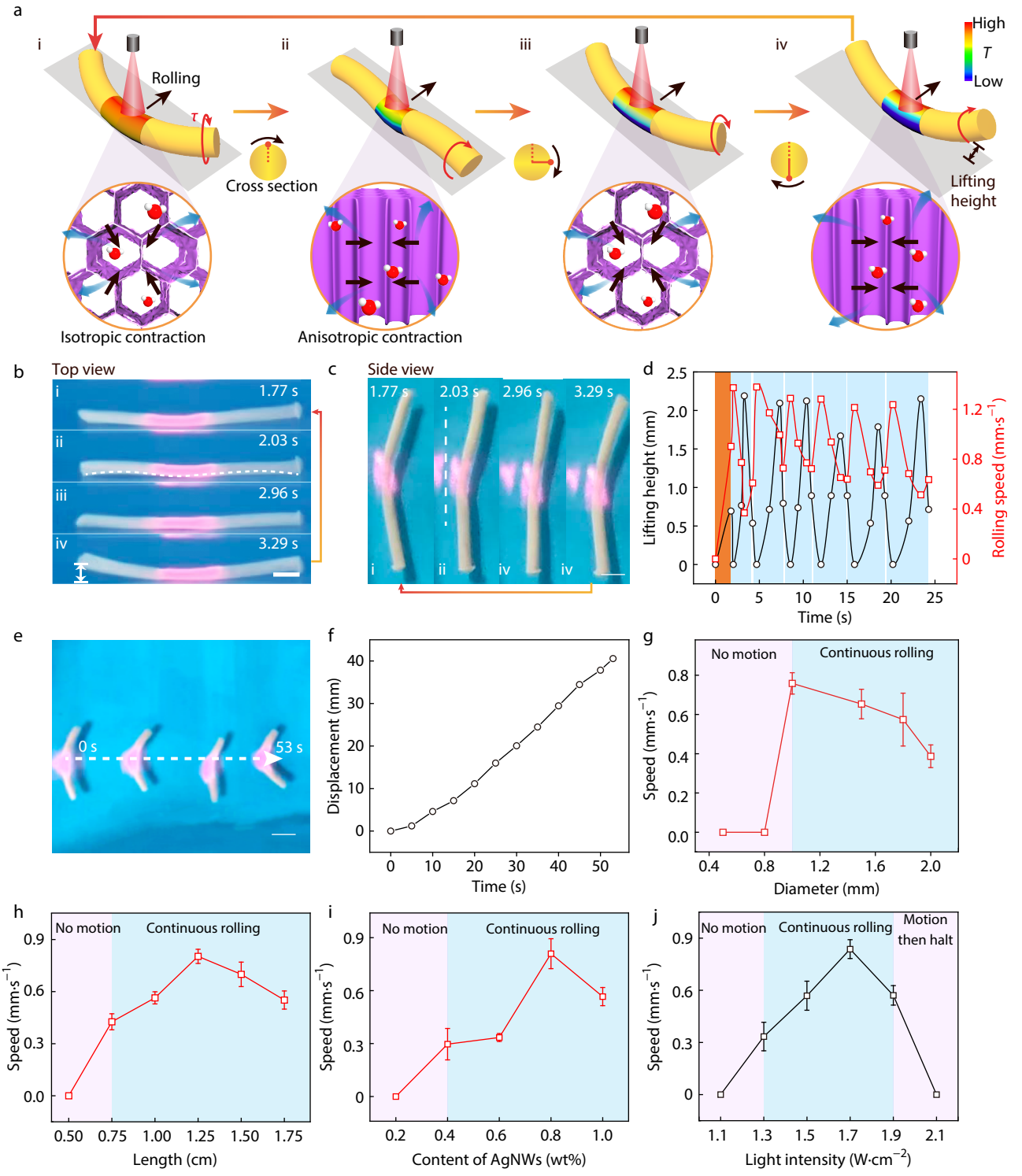

Fig. 3 Continuous self-rolling under constant light irradiation. (a) Schematic illustration of autonomous rolling mechanism; (b, c) Optical images of a rolling cycle under constant light stimulation from side view (b) and top view (c). Scale bar: 2 mm. (d) Variations of lifting height of the end and rolling speed of the APPA hydrogel as a function of time during rolling process. Orange and blue areas represented the initiation stage and the stable rolling stage, respectively. (e) Trajectory of the linear rolling motion. Scale bar: 5 mm. (f) Displacement of the APPA hydrogel actuator during linear rolling as a function of time under NIR irradiation at 1.7 W·cm^{-2}. (g–j) Effects of actuator diameter (g), length (h), AgNW content (i), and NIR light power density (j) on the autonomous rolling speed, respectively.

straight cylindrical hydrogel rolled randomly to the left or right under vertical light irradiation because of the inability to break the geometric symmetry (Fig. S16 in ESI).

It was found that the curved cylindrical APPA hydrogel ex-

perienced an initiation stage, followed by steady rolling at a nearly constant speed under continuous NIR light irradiation (Figs. 3b and 3c). Specifically, the phototropic bending induced by the photothermal gradient provided the driving moment for rolling, while the lifting height determined the recovery speed and rolling resistance of the hydrogel, thereby strongly coupling the deformation dynamics with the rolling state. Meanwhile, the honeycomb-like network and lamellar structure of the hydrogel exhibited distinct differences in the bending deformation magnitude under light illumination (Fig. S17 in ESI). Such deformation differences periodically broke the mechanical equilibrium of the system, maintaining a dynamic imbalance between the driving moment and the resistive torque. Ultimately, the lifting height at both ends and the instantaneous rolling speed of the hydrogel exhibited periodic oscillatory behaviors and opposite variation trends as a function of irradiation time (Fig. 3d). Under continuous light irradiation, the APPA hydrogel achieved a total distance of 41 mm at an average rolling speed of 0.77 $mm{\cdot}s^{-1}$ (Figs. 3e, 3f and Movie S1 in ESI). Impressively, although the IPPA hydrogel could achieve autonomous rolling, its rolling velocity was only 0.38 $mm{\cdot}s^{-1}$, much slower than that of the APPA hydrogel (Fig. S18 in ESI). This was because the anisotropic APPA hydrogel could effectively concentrate energy and generate a larger rolling torque, resulting in a higher rolling speed, whereas the IPPA hydrogel with an isotropic structure lacked energy concentration and large bending deformation. In contrast, the PA hydrogel with a disordered and dense polymer network failed to autonomously move because of the lack of rapid swelling-contraction ability (Fig. S19 in ESI).

The influences of geometric parameters, including diameter, length and curvature, on the self-rolling speed of the APPA hydrogel were explored. The rolling behavior was closely related to the gel diameter, which determined the establishment of cross-sectional temperature gradients. At a light intensity of 1.7 $W{\cdot}cm^{-2}$, the temperature difference between the irradiated and non-irradiated surfaces of gels with diameters smaller than 0.8 mm was less than 10 °C, resulting in insufficient differential shrinkage stress to induce bending deformation and thus preventing rolling (Fig. S20 in ESI). With increasing diameter, the cross-sectional temperature difference rose accordingly, yet an excessively large diameter increased the gel mass and moment of inertia, as reflected by a decrease in rolling speed from 0.76 $mm{\cdot}s^{-1}$ to 0.39 $mm{\cdot}s^{-1}$ (Fig. 3g). Furthermore, the rolling dynamics were regulated by the gel length. At a fixed light-spot area, a moderate increase in length facilitated the conversion of local shrinkage into larger net displacements, thereby improving the rolling speed. However, the excessive length introduced additional mass and resistance, hindering sustained rolling (Fig. 3h). The introduction of an appropriate curvature was intended to break the symmetry of the structure, thereby enabling controllable rolling under light irradiation. When the hydrogel without curvature was subjected to continuous vertical light irradiation, it exhibited random rolling to the left or right with a rolling speed of 0.8 mm^{-1} due to the uniform distribution of contractile strain caused by photothermal shrinkage. As the curvature increased, the self-rolling speed of the hydrogel decreased, which was primarily attributed to the enhanced energy barrier of photothermal deformation and reduction in available strains for movement (Fig. S21 in ESI).

Self-sustained rolling was associated with the input energy governed by the AgNW content and light intensity, which determined the driving force, speed, and sustainability of autonomous rolling by regulating the dynamic thermal balance. Specifically, the AgNW content determined the light absorption and photothermal conversion capability of the hydrogel, whereas the incident light intensity controlled the energy input flux into the system. At low light intensities (<1.3 $W{\cdot}cm^{-2}$) or insufficient AgNW content, the energy input was inadequate to generate the driving force required to initiate rolling. Increasing the AgNW content or light intensity within an appropriate range enhanced the response speed and optimized the spatial thermal distribution, resulting in an increase in rolling speed from 0.29 $mm{\cdot}s^{-1}$ to 0.81 $mm{\cdot}s^{-1}$ (Figs. 3i and 3j). Nevertheless, excessive AgNW content or intense light irradiation induced localized overheating in the illuminated region, which caused persistent shrinkage of the hydrogel and ultimately reduced its rolling speed.

In addition to linear rolling, controllable movement of the curved cylindrical hydrogel could be achieved by spatially modulating the irradiation region. When the irradiation spot deviated from the center, off-center photothermal heating induced an asymmetric contraction between the upper and lower regions of the hydrogel, thereby generating a steering torque that deflected the rolling trajectory (Movie S2 in ESI). As shown in Fig. 4(a), when a light spot was applied to the upper half of the hydrogel, the contraction region was concentrated in the upper portion. Under continuous light stimulation, the sustained deformation asymmetry between the upper and lower halves produced a persistent steering torque, driving the hydrogel to undergo autonomous anticlockwise turning. The corresponding *X*-*Y* trajectory exhibited a continuous lateral deflection, with the *Y* displacement increasing to about 20 mm over a forward distance of about 45 mm, confirming sustained steering under localized irradiation (Fig. 4b). Conversely, when the irradiation region was shifted to the lower half, the contraction was localized in the lower portion, resulting in an opposite torque that induced a clockwise turning motion, with the *Y* displacement decreasing from 0 mm to –16 mm over a forward displacement of about 30 mm within 72 s (Figs. 4c and 4d). Furthermore, we fabricated S-shaped and M-shaped hydrogels with anisotropic porous structures by unidirectional freezing-assisted UV photopolymerization. Under continuous NIR irradiation, the localized asymmetric strain at the bending node of the S-shaped hydrogel caused the two ends to detach from the substrate, enabling autonomous rolling through alternating contact with the underlying surface (Figs. S22a in ESI). Moreover, the M-shaped actuator with a sharp protrusion point exhibited vertical height fluctuations during locomotion and achieved efficient rolling displacement with larger strides by alternately landing on its two ends and protrusion point (Fig. S22b in ESI). These findings confirmed that the fabrication strategy could be extended to the construction of actuators with complex curvatures, offering a versatile route for designing self-rolling hydrogels with sophisticated asymmetric geometries.

https://doi.org/10.1007/s10118-026-3734-2

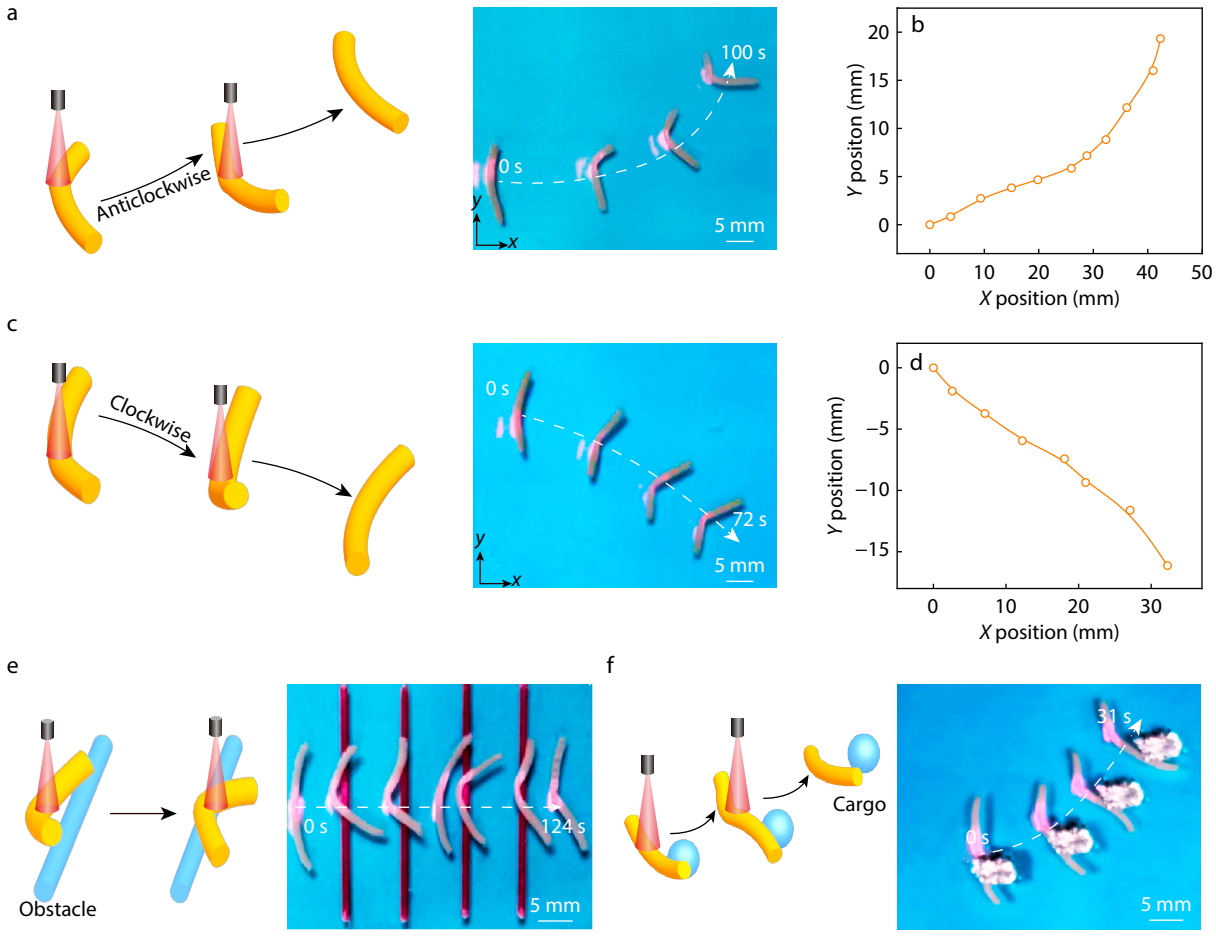

Fig. 4 Light-guided directional self-rolling and multifunctional applications. (a) Schematic diagram and optical image of autonomous anticlockwise steering motion induced by localized light irradiation on the upper half of the hydrogel; (b) Corresponding *X*-*Y* centroid trajectory of counterclockwise steering motion; (c) Schematic diagram and optical image of autonomous clockwise steering motion upon localized light irradiation on the lower half of the actuator; (d) Corresponding *X*-*Y* centroid trajectory of the clockwise steering motion; (e) Schematic diagram and optical image of autonomous hurdle crossing; (f) Schematic diagram and optical image of autonomous cargo transportation. NIR intensity, 1.7 W·cm^{-2}.

By leveraging programmable linear and steering motions, the actuation capabilities of the curved cylindrical hydrogel were further extended to complex tasks, including obstacle negotiation and cargo transport. Specifically, when the lifting height during the movement exceeded the height of the obstacle, the two ends of the hydrogel were supported by the obstacle, and the large-amplitude bending combined with instantaneous speed enabled the hydrogel to lift its body and traverse the obstacle, achieving continuous autonomous hurdle crossing (Fig. 4e and Movie S3 in ESI). Similarly, the hydrogel was capable of autonomous climbing. When the lifting height exceeded the step height, it could surmount the step and subsequently maintain stable rolling on the elevated surface, enabling a continuous climbing motion (Fig. S23 in ESI). Interestingly, when the lifting height was lower than the obstacle height, the two ends of the hydrogel failed to surmount the obstacle during downward motion. Instead, under continuous actuation, periodic contraction in contact with the obstacle generated a net horizontal reaction force through mechanical constraints and friction, resulting in forward displacement of the obstacle and enabling autonomous cargo transport (Fig. 4f). These multifunctional behaviors highlighted the effectiveness of integrating microscale anisotropic architectures with macroscopic geometric designs, providing a versatile strategy for autonomous soft robots operating in complex environments.

CONCLUSIONS

A facile strategy was developed to fabricate curved cylindrical hydrogels with aligned porous channels *via* directional freezing-assisted *in situ* photopolymerization, enabling directionally controllable autonomous rolling under constant light stimulation. Benefiting from the anisotropic structure and oriented open-cell network, the cylindrical hydrogel exhibited rapid anisotropic deformation, with a shrinkage ratio of 0.21 in the length direction within 2.1 s, which was 2 times higher than that in the diametral direction. Under light irradiation, the hydrogel rapidly bent to 48° within 2.9 s and fully recovered to its initial shape within 2 s upon removal of the light. Notably, with the coupling effect of the intrinsically oriented porous structure and geometric curvature, the hydrogel could realize continuous au-

https://doi.org/10.1007/s10118-026-3734-2

tonomous rolling under constant NIR light irradiation with a rolling speed of 0.77 mm·s^{-1}. Directionally controllable rolling could be achieved by spatially modulating the irradiated region. Furthermore, the hydrogel demonstrated multifunctional capabilities, including obstacle crossing, stair climbing, and cargo transport, under constant stimulation. This study provides a versatile platform for high-performance hydrogel actuators and offers new opportunities for the development of biomimetic intelligent soft robotic systems in complex environments.

Conflict of Interests

The authors declare no interest conflict.

Electronic Supplementary Information

Electronic supplementary information (ESI) is available free of charge in the online version of this article at http://doi.org/10.1007/s10118-026-3734-2.

Data Availability Statement

The data that supporting the results of this study are available from the corresponding author upon reasonable request. Contact information of the corresponding authors: hpcong@hfut.edu.cn (H.P.C.), xinyao@hfut.edu.cn (X.Y.)

ACKNOWLEDGMENTS

This work was financially supported by the National Natural Science Foundation of China (Nos. 22471052 and 22171066).

REFERENCES

1 Mou, F.; Chen, C.; Zhong, Q.; Yin, Y.; Ma, H.; Guan J. Autonomous motion and temperature-controlled drug delivery of Mg/Pt-poly(N-isopropylacrylamide) Janus micromotors driven by simulated body fluid and blood plasma. *ACS Appl. Mater. Interfaces* **2014**, *6*, 9897–9903.
2 Cecchini, L.; Mariani, S.; Ronzan, M.; Mondini, A.; Pugno, N. M.; Mazzolai, B. 4D printing of humidity-driven seed inspired soft robots. *Adv. Sci.* **2023**, *10*, 2205146.
3 Luo, D.; Maheshwari, A.; Danielescu, A.; Li, J.; Yang, Y.; Tao, Y.; Sun, L.; Patel, D. K.; Wang, G.; Yang, S.; Zhang, T.; Yao, L. Autonomous self-burying seed carriers for aerial seeding. *Nature* **2023**, *614*, 463–470.
4 Wang, T.; Jin, T.; Lin, W.; Lin, Y.; Liu, H.; Yue, T.; Tian, Y.; Li, L.; Zhang, Q.; Lee, C. Multimodal sensors enabled autonomous soft robotic system with self-adaptive manipulation. *ACS Nano* **2024**,

Graphical Abstract

Anisotropic Hydrogels with Aligned Porous Structures for Light-steerable Autonomous Rolling

Jia-Xin Yu, Xin Yao, Ru-Yu Zheng, and Huai-Ping Cong

Hefei University of Technology

A simple strategy was developed for the fabrication of curved cylindrical hydrogels with oriented porous structures that enabled autonomous rolling under constant light irradiation *via* directional freezing assembly-assisted *in situ* photopolymerization.

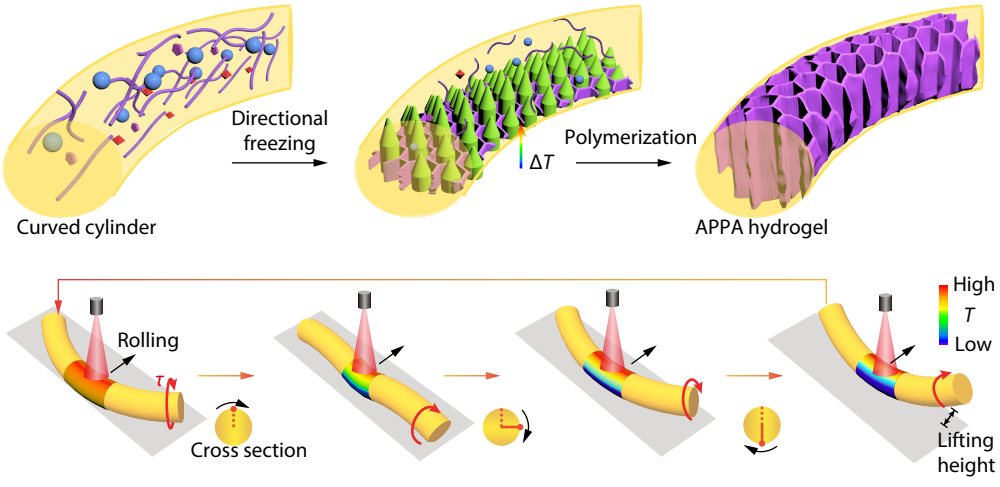

Chinese J. Polym. Sci., 2026 *https://doi.org/10.1007/s10118-026-3734-2*

18, 9980–9996.
5 He, Q.; Yin, R.; Hua, Y.; Jiao, W.; Mo, C.; Shu, H.; Raney, J. R. A modular strategy for distributed, embodied control of electronics-free soft robots. *Sci. Adv.* **2023**, *9*, eade9247.
6 Su, J.; Tan, J.; Liu, J.; He, K.; Wu, D.; Lai, W.; Cao, J.; Phee, S. J.; Magdassi, S.; Chen, X. Bioarchitectonics-inspired soft grippers with cutaneous slip perception. *Sci. Adv.* **2025**, *11*, eadx4206.
7 Yuk, H.; Lu, B.; Zhao, X. Hydrogel bioelectronics. *Chem. Soc. Rev.* **2019**, *48*, 1642–1667.
8 Drury, J. L.; Mooney, D. J. Hydrogels for tissue engineering: scaffold design variables and applications. *Biomater.* **2003**, *24*, 4337–4351.
9 Dai, C.; Zhu, Q.; Khoruzhenko, O.; Thelen, M.; Bai, H.; Breu, J.; Du, M.; Zheng, Q.; Wu, Z. Reversible snapping of constrained anisotropic hydrogels upon light stimulations. *Adv. Sci.* **2024**, *11*, 2402824.
10 Hua, M.; Kim, C.; Du, Y.; Wu, D.; Bai, R.; He, X. Swaying gel: chemo-mechanical self-oscillation based on dynamic buckling. *Matter* **2021**, *4*, 1029–1041.
11 Hou, G.; Zhang, X.; Du, F.; Wu, Y.; Zhang, X.; Lei, Z.; Lu, W.; Zhang, F.; Yang, G.; Wang, H.; Liu, Z.; Wang, R.; Ge, Q.; Chen, J.; Meng, G.; Fang, N. X.; Qian, X. Self-regulated underwater phototaxis of a photoresponsive hydrogel-based phototactic vehicle. *Nat. Nanotechnol.* **2024**, *19*, 77–84.
12 Sun, J.; Hu, W.; Zhang, L.; Lan, R.; Yang, H. Yang, D. K. Light-driven self-oscillating behavior of liquid-crystalline networks triggered by dynamic isomerization of molecular motors. *Adv. Funct. Mater.* **2021**, *31*, 2103311.
13 Gelebart, A. H.; Mulder, D. J.; Varga, M.; Konya, A.; Vantomme, G.; Meijer, E. W.; Selinger, R. L. B.; Broer, D. J. Making waves in a photoactive polymer film. *Nature* **2017**, *546*, 632–636.
14 Li, Z.; Myung, N. V.; Yin, Y. Light-powered soft steam engines for self-adaptive oscillation and biomimetic swimming. *Sci. Robot.* **2021**, *6*, eabi4523.
15 Zhu, Q.; Liu, W.; Khoruzhenko, O.; Breu, J.; Bai, H.; Hong, W.; Zheng, Q.; Wu, Z. Closed twisted hydrogel ribbons with self-sustained motions under static light irradiation. *Adv. Mater.* **2024**, *36*, 2314152.
16 Zhao, Y.; Xuan, C.; Qian, X.; Alsaid, Y.; Hua, M.; Jin, L.; He, X. Soft phototactic swimmer based on self-sustained hydrogel oscillator. *Sci. Robot.* **2019**, *4*, eaax7112.
17 Guo, K.; Yang, X.; Zhou, C.; Li, C. Self-regulated reversal deformation and locomotion of structurally homogenous hydrogels subjected to constant light illumination. *Nat. Commun.* **2024**, *15*, 1694.
18 Yang, Y.; Li, C.; Palmer, L. C.; Stupp, S. I. Autonomous hydrogel locomotion regulated by light and electric fields. *Sci. Adv.* **2023**, *9*, eadi4566.
19 Dawson, C.; Vincent, J. F. V.; Rocca, A. M. How pine cones open. *Nature* **1997**, *390*, 668.
20 Reed, R.; Houston, T. W.; Todd, P. M. Structure and function of the sarcolemma of skeletal muscle. *Nature* **1966**, *211*, 534–536.
21 Žižka, Z. Anisotropic structures of some microorganisms studied by polarization microscopy. *Folia Microbiol.* **2014**, *59*, 363–368.
22 Yan, Q.; Ding, R.; Zheng, H.; Li, P.; Liu, Z.; Chen, Z.; Xiong, J.; Xue, F.; Zhao, X.; Peng, Q.; He, X. Bio-inspired stimuli-responsive $Ti_3C_2T_x$/PNIPAM anisotropic hydrogels for high-performance actuators. *Adv. Funct. Mater.* **2023**, *33*, 2301982.
23 Yao, X.; Chen, H.; Qin, H.; Wu, Q. H.; Cong, H. P.; Yu, S. H. Solvent-adaptive hydrogels with lamellar confinement cellular structure for programmable multimodal locomotion. *Nat. Commun.* **2024**, *15*, 9254.
24 Zhang, Y.; Yao, X.; Yu, J.; Qin, H.; Cong, H. P. Gradient crosslinking of anisotropic hydrogels for programmable shape morphing and actuation. *Chin. Chem. Lett.* **2026**, *37*, 112041.
25 Kim, D. S.; Lee, Y.-J.; Kim, Y. B.; Wang, Y.; Yang, S. Autonomous, untethered gait-like synchronization of lobed loops made from liquid crystal elastomer fibers *via* spontaneous snap-through. *Sci. Adv.* **2023**, *9*, eadh5107.
26 Zhu, Q.; Liu, W.; Khoruzhenko, O.; Breu, J.; Hong, W.; Zheng, Q.; Wu, Z. Animating hydrogel knotbots with topology-invoked self-regulation. *Nat. Commun.* **2024**, *15*, 300.
27 Zhu, Q.; Cheng, H.; Liu, W.; Xiao, Y.; Wu, X.; Breu, J.; Hong, W.; Wang, Z.; Zheng, Q.; Wu, Z. Light-driven self-sustained rolling of cylinder hydrogels with fast and anisotropic responses. *Chinese J. Polym. Sci.* **2025**, *43*, 548–555.
28 He, X.; Sun, Y.; Wu, J.; Wang, Y.; Chen, F.; Fan, P.; Zhong, M.; Xiao, S.; Zhang, D.; Yang, J.; Zheng, J. Dual-stimulus bilayer hydrogel actuators with rapid, reversible, bidirectional bending behaviors. *J. Mater. Chem. C* **2019**, *7*, 4970–4980.
29 Fan, W.; Shan, C.; Guo, H.; Sang, J.; Wang, R.; Zheng, R.; Sui, K.; Nie, Z. Dual-gradient enabled ultrafast biomimetic snapping of hydrogel materials. *Sci. Adv.* **2019**, *5*, eaav7174.
30 Shang, M.; Ma, S.; Ma, J.; Guo, L.; Liu, C.; Xu, X. Somatosensory actuators based on light-responsive anisotropic hydrogel for storage encryption of information systems. *Chem. Eng. J.* **2024**, *496*, 153895.
31 Lu, Y.; Li, S.; Ma, Y.; Deng, F.; Yue, Y.; Jiang, S.; Ye, M.; Zhou, Y.; Xiao, H.; Han, J. Nanocellulose-assisted construction of conductive gradient hydrogel for remote actuated and self-sensing soft actuator. *Carbohydr. Polym.* **2025**, *368*, 124092.
32 Tan, Y.; Wang, D.; Xu, H.; Yang, Y.; Wang, X.-L.; Tian, F.; Xu, P.; An, W.; Zhao, X.; Xu, S. Rapid recovery hydrogel actuators in air with bionic large-ranged gradient structure. *ACS Appl. Mater. Interfaces* **2018**, *10*, 40125–40131.
33 Tan, Y.; Wang, D.; Xu, H.; Yang, Y.; An, W.; Yu, L.; Xiao, Z.; Xu, S. A fast, reversible, and robust gradient nanocomposite hydrogel actuator with water-promoted thermal response. *Macromol. Rapid Commun.* **2018**, *39*, 1700863.
34 Gao, Y.; Zhao, X.; Han, X.; Wang, P.; Zheng, W. Soft actuator based on metal/hydrogel nanocomposites with anisotropic structure. *Macromol. Chem. Phys.* **2022**, *223*, 2100117.